Cerebral Cortex January 2010;20:229–240
doi:10.1093/cercor/bhp093
Advance Access publication May 15, 2009

Neurotrophin-3 Is Involved in the Formation of Apical Dendritic Bundles in Cortical Layer 2 of the Rat

Toshio Miyashita[1,3], Marie Wintzer[1], Tohru Kurotani[1], Tomokazu Konishi[2], Noritaka Ichinohe[1] and Kathleen S. Rockland[1]

[1]Laboratory for Cortical Organization and Systematics, RIKEN Brain Science Institute, 2-1 Hirosawa, Wako-shi, Saitama 351-0198, Japan and [2]Faculty of Bioresource Sciences, Akita Prefectural University, Shimo-Shinjyo, Akita 010-0195, Japan

[3]Current address: Department of Molecular and Cell Biology, Helen Wills Neuroscience Institute, University of California at Berkeley, Berkeley, CA 94720, USA

Apical dendritic bundles from pyramidal neurons are a prominent feature of cortical neuropil but with significant area specializations. Here, we investigate mechanisms of bundle formation, focusing on layer (L) 2 bundles in rat granular retrosplenial cortex (GRS), a limbic area implicated in spatial memory. By using microarrays, we first searched for genes highly and specifically expressed in GRS L2 at postnatal day (P) 3 versus GRS L2 at P12 (respectively, before and after bundle formation), versus GRS L5 (at P3), and versus L2 in barrel field cortex (BF) (at P3). Several genes, including *neurotrophin-3* (*NT-3*), were identified as transiently and specifically expressed in GRS L2. Three of these were cloned and confirmed by in situ hybridization. To test that NT-3–mediated events are causally involved in bundle formation, we used in utero electroporation to overexpress *NT-3* in other cortical areas. This produced prominent bundles of dendrites originating from L2 neurons in BF, where L2 bundles are normally absent. Intracellular biocytin fills, after physiological recording in vitro, revealed increased dendritic branching in L1 of BF. The controlled ectopic induction of dendritic bundles identifies a new role for NT-3 and a new in vivo model for investigating dendritic bundles and their formation.

Keywords: dendrite, electroporation, GeneChip, minicolumns, pyramidal neuron

Introduction

Apical dendrites of cortical pyramidal neurons commonly form bundles (Feldman and Peters 1974; Fleischhauer 1974; Escobar et al. 1986; Peters and Kara 1987). These have been considered as an important feature of cortical microcircuitry although their spatial compartmentalization as well as functional implications remain unclear (Mountcastle 1997, 2003; Jones 2000; Rockland and Ichinohe 2004; DeFelipe 2005; Krieger et al. 2007). A potentially useful model system for investigating dendritic bundles is rat granular retrosplenial cortex (GRS), a limbic area associated with spatial navigation and interconnected with the hippocampal formation (Wyss and Van Groen 1992; Cooper and Mizumori 2001; Harker and Whishaw 2002; Miyashita and Rockland 2007). The GRS has prominent apical dendritic bundles in layer (L) 1, which derive from callosally projecting pyramidal neurons in L2, are specifically targeted by thalamic input from the anterior ventral and dorsal nuclei (Wyss et al. 1990), and interdigitate with a second system of dendritic bundles from deeper pyramidal neurons in L3 and L5 (Ichinohe, Yoshihara, et al. 2003).

In a previous study (Ichinohe, Yoshihara, et al. 2003), we reported that L2 bundles in the GRS (so designated because of their origin from L2 pyramidal neurons) are detectable from postnatal day (P) 5 and provided evidence that bundle formation involves a repellant influence of OCAM, a cell adhesion molecule located on the dendritic surface of L5 neurons. In order to identify other candidate molecules involved in bundle formation, we here used microarrays to screen for highly expressed genes in L2 of the GRS at P3 (before bundle formation). In particular, to assess specificity, we compared gene expression profiles by layer at P3 (GRS L2 vs. L5), by area at P3 (GRS L2 vs. L2 of barrel cortex), and by stage (P3 vs. P12 of GRS L2). This screening identified *neurotrophin-3* (*NT-3*) as highly and specifically expressed in the GRS L2 at P3.

To test the importance of NT-3–mediated events in bundle formation, we used in utero electroporation to overexpress *NT-3* in cortical areas where L2 bundles are normally absent. This intervention in fact successfully induced apical dendritic bundling in barrel cortex and adjacent regions. Finally, morphometric analysis of single cells, intracellularly filled with biocytin in slice preparations from *NT-3* overexpressed barrel cortex, demonstrated increased dendritic branching in L1. The increased branching is consistent with known effects of NT-3 (McAllister et al. 1995; Catapano et al. 2004). These results begin to identify the multiple molecular mechanisms underlying bundle formation and offer a new model system for investigating area-specific cortical structural plasticity.

Materials and Methods

Laser Microdissection and GeneChip Hybridization

Total RNA was extracted from 4 male Wistar rat pups (P3 and P12; 2 animals at each age). All experimental procedures described here were approved by the Experimental Animal Committee of the RIKEN Institute and were carried out in accordance with institutional guidelines. Every effort was made to minimize the number of animals used.

After decapitation, nonfixed brains were dissected, immediately frozen with powdered dry ice, and stored at −80 °C until used. Coronal brain sections (10 μm) containing the S1 barrel field cortex (BF) and GRS were cut by cryostat and mounted on Leica foil slides (Leica Microsystems, Wetzlar, Germany). After sectioning, slides were stored immediately at −80 °C until further use. On the day of laser microdissection (LMD), the slides were removed from the freezer, fixed in ice-cold 95% ethanol (EtOH)/5% acetic acid solution for 3 min, and then rinsed with ice-cold Diethylpyrocarbonate-treated H_2O (DEPC-H_2O). Slides were stained with 0.05% toluidine blue for 30 s, rinsed twice with ice-cold DEPC-H_2O, and then air-dried. L2 and L5 from both GRS and BF at the 2 different developmental stages (P3 and P12) were laser microdissected (Fig. 1) on a Leica AS LMD system (Leica Microsystems). About 30–40 tissue fragments were collected from each brain site. These are roughly equal to 1–5 × 10^6 μm^2. These fragments were directly collected in 50 μL of the RLT buffer of RNeasy

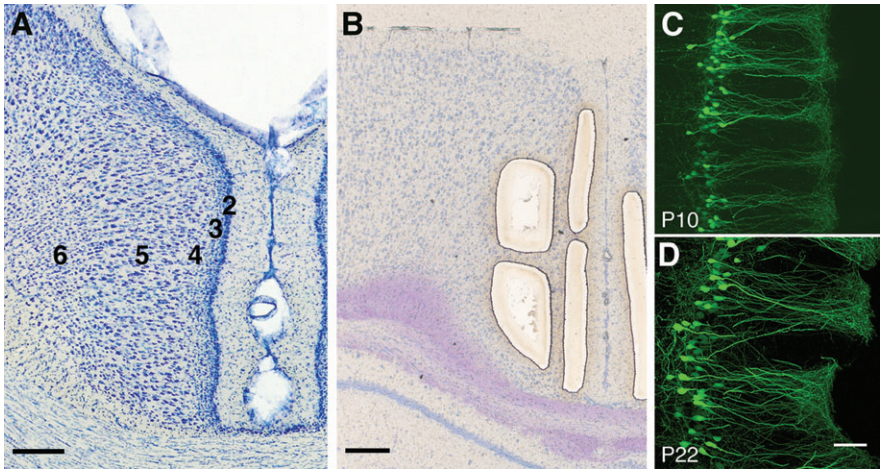

Figure 1. GRS cortex, left hemisphere of rat. (*A*) Coronal section (thionin stain for cell bodies) of adult GRS from around bregma −4.0 mm. (B) Toluidine blue–stained, unfixed section (P28 rat). L2 and L5 were excised by LMD (Leica Microsystems) for RNA extraction. (*C*, *D*) Dendritic bundles in L1 (P10 in *C*, P22 in *D*), visualized by electroporation of *EGFP* at E18. Arabic numbers indicate layers. Scale bars = 200 μm in *A*, 250 μm in *B*, 50 μm in *D*, for *C* and *D*.

micro kit (Qiagen, Valencia, CA), and total RNA was extracted according to the manufacturer's instruction and eluted with 14 μL of DEPC-H_2O. Quality and quantity of extracted total RNA were checked by analyzing 1 μL of RNA on the Agilent Bioanalyzer with a picokit (Agilent Technology, Santa Clara, CA). We used only those tissue samples for which total RNA was measured as having an RNA integrity number ⩾ 7.0 (Supplementary Table S1).

Ten microliters (37–140 ng) of total RNA was used as input in the MessageAmp aRNA kit (Ambion, Foster City, CA) and amplified linearly. One microgram of amplified RNA was used as input for a second linear amplification in the MessageAmp Biotin Enhance II aRNA Kit (Ambion). Amplified and biotin-labeled RNA was fragmented according to manufacturer's instructions. Quality and quantity of amplified RNA from both the first and second round of linear amplification, and fragmented RNA, were analyzed on Agilent Bioanalyzer with a nanokit (Agilent Technology).

A total of 20 μg of biotin-labeled amplified RNA fragments were used as probes and hybridized to Rat Expression 230 2.0 Array (Affymetrix, Santa Clara, CA). These arrays contain 31 099 genes spanning the rat genome. Hybridization and scanning were performed as described by Affymetrix.

Microarray Data Analysis

Eight GeneChip arrays (rat 230 2.0) were used in this study. Raw image files were converted to probe signal value files by Microarray Analysis Suite (Affymetrix). Normalization of the perfect match (PM) intensities in each chip was performed by Skylight Biotech Inc (http://www.super-norm.com/eng/), and areas affected by dust in the hybridization were removed (Konishi 2006), according to a 3-parameter log normal distribution model (Konishi 2004). To avoid any effect of additive noise and saturation from the detection process, only signals in the model-coincident intensity range were used for further analysis. The expression levels of each gene were estimated by summarizing the corresponding PM data by the trimmed mean method (Konishi 2008).

Selection of Genes Specifically Expressed in GRS L2 at P3

Expression levels of genes were compared in a pairwise manner between GRS L2 at P3 and: the GRS L5 at P3 (comparison by layer), BF L2 at P3 (comparison by area), and GRS L2 at P12 (comparison by age). To minimize influences of individual variations that are not concerning to the cell differentiations, the comparisons by layer and area were repeatedly performed within the same rat's data rather than between groups simultaneously (see Konishi 2008, supplement "clustering"). To maintain this calculation framework, comparison by age was also repeatedly performed between pairwise data. Positive genes were selected by the following 3 steps.

Step 1: Genes that showed significant difference in expression levels were selected. In a data set, each level is measured using several PM cells, which have unique nucleotide sequence and position in a chip surface. The significance can be tested by comparing the average of expressional differences among the PM cells, and the noise level can be estimated by the deviations of the differences. Accordingly, between the pairs of chip data, corresponding normalized PM data of each gene were subjected to Welch's paired 2-sided *t*-test. A difference with $P < 0.01$ in both the pairs simultaneously was considered significant. Because the chip covers 31 099 genes, the maximum expectation value of false positives for each comparison is 3.1 (=31 099 × 0.01 x 0.01).

Step 2: Among the selected genes at step 1, those expressed more than 2 times in GRS L2 at P3, compared with the 3 other tissue samples, were again selected out.

Step 3: A final selection was carried out on the basis of reproducibility between 2 animals. Among genes selected at step 2, differences between the average of each tissue pair were subjected to Welch's *t*-test ($P < 0.05$). By this means, we eliminated within-group variations.

Riboprobe Preparation and In Situ Hybridization

Sense and antisense RNA probes were synthesized using a digoxigenin (DIG)–RNA labeling kit with SP6 or T7 RNA polymerase (Roche Diagnostics, Basel, Switzerland). Wistar rat pups (P3 and P12) of either sex were used for in situ hybridization. Pups were anesthetized with sodium pentobarbital injected intraperitoneally (Nembutal; 50 mg/kg of body weight) and perfused transcardially, in sequence, with 0.9% saline and 0.5% sodium nitrite for 1 min and 4% paraformaldehyde (PFA) in 0.1 M phosphate buffer (PB, pH 7.4) for 10 min. Postfixation was in the same fixative for 2 h. Then, the brains were immersed into 30% sucrose for cryoprotection (20–40 h at 4 °C) and cut into 30-μm-thick coronal sections on a freezing microtome. Sections were immediately mounted on MAS-coated slides (Matsunami, Osaka, Japan). In situ hybridization was carried out on slide-mounted histological sections, by standard methods (Miyashita et al. 2005). Finally, sections were incubated in nitro-blue tetrazolium chloride (NBT)/5-Bromo-4-Chloro-3′-Indolylphosphatase p-Toluidine salt (BCIP) solution (Roche Diagnostics) until adequate color development was achieved. No signals were observed when sections were processed with DIG-labeled sense RNA probes.

5-Bromo-2′-Deoxyuridine Incorporation and Immunohistochemistry

5-Bromo-2′-deoxyuridine (BrdU) was administered to 3 pregnant rats (20 mg/kg in physiological saline; intraperitoneal) at 17, 18, or 19 days

postcoitum (dpc). Pups were born by natural delivery and reared until P16, and then 3 pups from each mother rat were perfused as described above. Free-floating sections (50-μm thickness) from these brains were treated with 2 N HCl in distilled water (30 min) and then with 0.1 M sodium tetraborate (5 min). Sections were rinsed in 0.1 M PB twice (10 min), incubated for 1 h in 0.1 M phosphate-buffered saline (PBS) containing 0.5% Triton X-100 and 5% normal goat serum (PBS-TG) at room temperature (RT), and incubated for 40–48 h at 4 °C with primary mouse anti-BrdU antibody (BD Bioscience, San Jose, CA; 1:50). After rinsing with PBS, the sections were placed in PBS-TG containing biotinylated goat anti-mouse IgG (Vector, Burlingame, CA; 1:200) for 90 min at RT, and immunoreactivity (ir) was visualized by avidin–biotin complex incubation (one drop of reagents per 7 ml of 0.1 M PB, ABC Elite kits; Vector), followed by diaminobenzidene (DAB) histochemistry with the addition of 0.03% nickel ammonium sulfate. Some sections were counterstained with thionin to identify laminar structure.

Plasmid Construction

pCAG-NT3 plasmid for in utero electroporation was constructed in the following steps. Polymerase chain reaction (PCR) amplification was performed using pGEM-T-NT3 plasmid DNA as a template with the following set of oligonucleotide primers: 5′XhoNtf3, 5′-ATC TTA CTC GAG AAC AAG GTG **ATG** TCC-3′, and 3′XhoNtf3, 5′-ATA TCT CGA GAC AGA TGC CAA TTC ATG-3′ (underlines indicate the *Xho*I site used for further construction, and bold indicates translation start site). The amplified DNA fragment was subcloned into pGEM-T Easy Vector (Promega, Madison, WI) to generate pGEM-XhoNT3. The pCAG-NT3 was created by subcloning the *Xho*I fragment of pGEM-XhoNT3 into the *Xho*I site of pCAGGS vector (Niwa et al. 1991).

This plasmid was electroporated together with enhanced green fluorescent protein *(EGFP)* cDNA (pCAG-EGFP; kind gift from Dr Y. Hatanaka; Hatanaka et al. 2004).

In Utero Electroporation

Pregnant Wistar rats (18 dpc) were anesthetized with sodium pentobarbital intraperitoneally (Nembutal; 50 mg/kg of body weight) and then subjected to abdominal incision to expose the uterus. Through the uterine wall, embryos were visualized, and plasmids (0.5–2.0 μg/μL for each) were injected into the lateral ventricle through a glass capillary. Electric pulses were delivered to embryos by gently clasping their heads with forceps-shaped electrodes (CUY650-5; NEPA GENE, Ichikawa, Japan), connected to a square pulse electroporator (CUY21SC; NEPA GENE). Five 50-V pulses of 50 ms were applied at 950-ms intervals. Uterine horns were repositioned into the abdominal cavity, and the abdominal wall and the skin were sutured. Animals were recovered, and their pups were born by natural delivery. Pups were reared until different postnatal stages and then perfused as described above.

Immunofluorescent Staining

Free-floating sections (40-μm thickness) were incubated for 1 h in PBS-TG at RT. Then, the sections were incubated for 40–48 h at 4 °C with primary antibody (rabbit anti-vesicular glutamate transporter 2 [VGluT2]; SYSY, Gottingen, Germany; 1:1000; or mouse anti-parvalbumin [PV]; Swant, Bellinzona, Switzerland; 1:5000; or mouse anti-microtubule associated protein 2 [MAP2]; Chemicon, Temecula, CA; 1:1000). After rinsing with PBS, the sections were placed in PBS-TG containing fluorescently labeled secondary antibodies (Alexa 594–conjugated anti-rabbit IgG; Invitrogen, Carlsbad, CA, for VGluT2, or Alexa 594–conjugated anti-mouse IgG; Invitrogen, for PV and MAP2, 1:200).

Fluorescently labeled tissue sections were scanned by confocal microscopy (TCS SP2 AOBS, Leica Microsystems). Confocal scanning with *z*-axis depth was done by using a 40× oil immersion objective lens (for Alexa 488: Ar–Kr laser, excitation wave length 488 nm; and for Alexa 594: orange He–Ne laser, excitation wave length 594 nm). Scanned sequential optical sections were merged in a single maximum projection image.

Light and fluorescent microscope photographs were taken on digital cameras (Axioscop2 and Axiocam; Carl Zeiss Vision, Munchen-Hallbergmoos, Germany). Size, brightness, and contrast of images were adjusted over the whole frame by using Photoshop software (Adobe Systems, San Jose, CA), and no part of a frame was enhanced or modified in any way.

Patch Clamp Recording and Intracellular Fills

Both normal and *NT-3*–electroporated (at E18) Wistar rats were used. Rats at P24–27 were deeply anesthetized with isoflurane and decapitated. The brain was quickly removed and immersed into chilled and oxygenated (95% O_2 and 5% CO_2) artificial cerebrospinal fluid (ACSF) containing (in mM): NaCl 126, KCl 3, NaH_2PO_4 1.2, $MgSO_4$ 1.3, $CaCl_2$ 2.4, $NaHCO_3$ 26, and glucose 10. Coronal slices (300-μm thickness) were prepared from BF using a pro-7 vibrating microtome (Dosaka, Kyoto, Japan). After cutting, the slices were transferred to an interface-type chamber and perfused with oxygenated ACSF at 32–34 °C for at least 1 h for recovery. Then, one of the slices was placed in a recording chamber continuously perfused with oxygenated ACSF (2 mL/min) at 27–30 °C. EGFP-expressing neurons in L2 of BF were identified by fluorescent microscopy. In control BF, neurons in L2 were selected by laminar location and soma shape, by using infrared differentiation interference contrast video microscopy (BX-50; Olympus, Tokyo, Japan). Whole-cell recordings were conducted with borosilicate patch pipettes (BF150-110-10; Sutter Instrument, Novato, CA), filled with an internal solution containing (in mM): KCl 150, NaCl 10, $MgSO_4$ 5, 4-(2-hydroxyethyl)-1-piperazineethanesulfonic acid 10, and ethyleneglycol-bis(2-aminoethylether)-N,N,N′,N′-tetra acetic acid 0.3, with 3 mg/mL biocytin and pH 7.3 adjusted with KOH. Current clamp recordings were made by an Axoclamp 2B amplifier (Molecular Devices Corp, Sunnyvale, CA), and intrinsic membrane properties were examined by injecting step currents (duration, 1 s; amplitude, ±50–500 pA). After recording, the cells were filled with biocytin by diffusive loading through the patch pipette for 10–15 min. The patch pipette was slowly retracted from the cell after filling, so that the cell membrane was successfully resealed. In one slice, 1–6 neurons were filled, and then the slice was transferred back to the interface-type chamber for more than 1 h to assure complete transport of biocytin throughout the neurons. Slices were fixed with 4% PFA overnight at 4 °C, and biocytin-filled neurons were visualized by using fluorescently labeled streptavidin. Slices were rinsed in 0.1 M PB twice (10 min), incubated for 1 h in PBS-TG at RT, and incubated for 40–48 h at 4 °C with Alexa 594–conjugated streptavidin (Invitrogen). After rinsing with PBS, slices were mounted on slide glass and scanned by confocal microscopy (TCS SP2 AOBS).

Morphometric Analysis

The dendritic morphology of fluorescently labeled pyramidal neurons was analyzed by 2 methods. First, the number of dendrites that extend into L1a and the depth of the parent soma were measured with Image J software (http://rsb.info.nih.gov/ij/; National Institutes of Health, Bethesda, MD) from stacked confocal images. Results were mapped in scatter plots. Second, sequential confocal images of fluorescently labeled pyramidal neurons were traced using Neurolucida (MicroBrightField Inc, Colchester, VT). Sholl analysis of the number of dendritic intersections was performed by using NeuroExplorer (MicroBrightField Inc).

Results

Genes Specific to GRS L2 at P3

In the first 2 postnatal weeks, the cerebral cortex, including the GRS, undergoes dramatic maturational changes and structural remodeling. To determine the molecular basis of dendritic bundle formation in the GRS L2, we investigated the degree and time course of the gene expression changes by using microarray. Because we were interested in the formation and specialization of L2 bundles in the GRS, we screened the genes

that are highly and specifically expressed in GRS L2 at P3 (predating the formation of dendritic bundles; Supplementary Fig. S1). Any influences by additive noise of measurement or dust contamination were avoided at the stage of data normalization by using *t*-test on PM data (see Materials and Methods: Microarray Data Analysis). We carried out a 3-way comparison of gene expression level by layer, area, and stage and selected genes by 3 steps (see Materials and Methods: Selection of Genes Specifically Expressed in GRS L2 at P3). At the first step of gene selection, 1326 genes were selected as significantly different in all the 3 comparisons (the list of the data is available upon request). In the next step, genes expressed more than 2-fold higher in GRS L2 at P3 were selected. Comparison by stage (GRS L2 at P3 vs. P12) resulted in a list of 306 genes; comparison by layer (GRS L2 vs. GRS L5, at P3) resulted in 107 genes; and comparison by area (L2 GRS vs. L2 BF, at P3) resulted in 173 genes (lists of the expression levels are in the Supplementary Tables S2–S4). Among those 3 groups of genes, 21 genes were common to all 3 comparisons.

Table 1
List of 12 genes selected by steps 1–3

	Affymetrix probe set ID	Genbank accession number	Expression level in P3 GRS L2 (*z* score)	Fold change P3 GRS L5	Fold change P3 BF L2	Fold change P12 GRS L2	Average fold change	Gene symbol
1	1387267_at	NM_031073	1.81	37.5	36.6	8.0	22.2	Ntf3
2	1376458_at	BE114418	1.04	6.8	7.3	8.8	7.6	*5HTr1a*[a]
3	1368080_at	NM_054008	1.42	4.0	11.3	4.2	5.7	Rgc-32
4	1395052_at	BE118917	1.38	2.1	14.8	4.7	5.3	
5	1393547_at	BE101549	1.80	3.0	3.4	12.9	5.1	Rnf182
6	1398412_at	BF402250	1.71	2.9	4.1	11.0	5.1	
7	1369167_at	NM_012750	1.39	3.5	13.2	2.6	5.0	Gfra2
8	1370570_at	AF016296	1.65	2.8	11.7	3.3	4.7	Nrp1
9	1377064_at	AI602811	1.37	3.0	10.5	2.3	4.2	Dusp6
10	1376066_at	AI103572	1.37	2.5	4.3	6.2	4.1	*Rnd3*[a]
11	1377663_at	AI598323	1.38	2.4	3.9	5.4	3.6	Rnd3
12	1385068_at	BF397283	0.88	3.8	3.0	2.8	3.2	

Note: Genes are listed by average fold change levels. Comparisons were made between P3 GRS L2 and 3 different tissue samples.
[a]No annotations were obtained from Affymetrix database, but BLAST homology search showed high similarities for these genes.

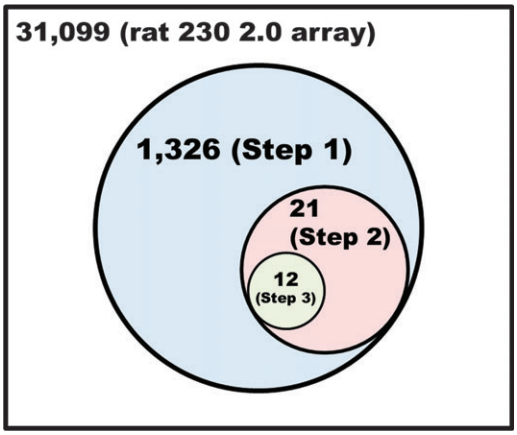

Figure 2. A 3-step selection of positive genes was applied to a total of 31 099 genes. Step 1: genes that showed a significantly different expression level in all the 3 comparisons (1326 genes). Step 2: genes whose expression was 2 times greater in GRS L2 at P3, compared with the 3 other tissue samples (21 genes). Step 3: reproducibility between 2 animals (12 genes).

After examining for biological reproducibility (step 3), 12 genes of interest remained (see scatter plot in Supplementary Fig. S2 and Supplementary Table S5), from the initial total of 31 099 genes (Table 1, Fig. 2, Supplementary Fig. S3). These included 5 genes without annotation in the Affymetrix database, but 2 of these showed high similarity to known genes (*5HTr1a* and *Rnd3*; see Table 1), whereas Basic Local Alignment Search Tool (BLAST) search showed no matching gene for the other 3. Among these 12 genes, the list included several genes potentially related to neural development in various ways, such as *Gfra2* (glial cell line–derived neurotrophic factor family receptor alpha; receptor for neurotrophic factor), dual-specificity phosphatase 6 (*DUSP6*), *Rnd3* (intracellular signaling molecules), and the *NT-3* (neurotrophic factor). *NT-3*, however, showed the most distinctive difference from the average among these 12 genes in GRS L2 at P3 and the greatest area and layer expression differences (36.6 times higher than BF L2 at P3 and 37.5 times higher than GRS L5 at P3). Developmental stage differences were less marked, although NT-3 expression at P3 is 8 times higher than at P12 (Table 1, Supplementary Fig. S3).

Confirmation of Gene Expression Patterns by In Situ Hybridization

With the goal of validating the microarray data and further pinpointing candidate genes that might be involved in bundle formation, we selected 3 genes including *NT-3*, cloned these by reverse transcription polymerase chain reaction (RT-PCR), and carried out in situ hybridization. We confirmed that the specificity by stage, layer, and area was identical to that reported by microarray analysis (Fig. 3). Of these 3 genes, *NT-3* was most intensely expressed in the GRS in L2 at P3 (preceding bundle formation) and showed the largest decrease between P3 and P12 (after bundle formation). Its expression level was significantly lower in BF (Table 1). For *Rnd3*, in addition to L2 expression, there was weak expression in L5 at P3. The expression level decreased in both layers at P12. At P12, a few scattered cells were stained with *Rnd3* probes, the distribution of which (i.e., all layers, including L1) is suggestive of γ-aminobutyric acidergic (GABAergic) neurons. At P12, *Rgc-32* also showed some scattered cells, larger in number than the *Rnd3*-positive cells. (Badea et al. 1998 identify *Rgc-32* expression in oligodendrocytes).

Because both the microarray and in situ hybridization data revealed strong expression of *NT-3* at an appropriate stage and site for bundle formation in the GRS, our next step was to more directly test its role in dendritic bundle formation. For this purpose, we chose to overexpress *NT-3* by in utero electroporation.

L2 Dendritic Bundles Induced by Ectopically Expressed NT-3

BF has a well-developed modularity in L4 and distinct bundles of L5 apical dendrites (Escobar et al. 1986; White and Peters 1993; Krieger et al. 2007) but no distinct bundling of L2 apical dendrites in the normal rat. Moreover, in the normal condition, *NT-3* is expressed at low levels in BF (Table 1 and Friedman et al. 1991). Accordingly, we targeted L2 of BF to overexpress *NT-3*.

Injection of EGFP expression plasmid into the lateral ventricle followed by electroporation specifically labels cortical

neurons in a birthday-dependent manner (Saito and Nakatsuji 2001; Tabata and Nakajima 2001; Hatanaka and Murakami 2002; Hatanaka et al. 2004). Uptake of BrdU between embryonic days 17–19 (E17–E19) and subsequent immunohistochemistry established that E18 is the major generational epoch for L2 pyramidal neurons in BF (as well as in other neocortical areas; data not shown and Lucio et al. 1997; Berbel et al. 2001).

With this information, we carried out controls by electroporation of EGFP alone at E18 in BF and GRS. This resulted in replication of the normal phenotype for each area; namely, EGFP-expressing neurons in BF but without distinct bundles (Fig. 4*A*) and in GRS EGFP-expressing neurons whose dendrites formed prominent bundles (Fig. 1*C,D*, Supplementary Fig. S1).

After electroporation (E18) of *NT-3* with EGFP in BF, abundant and apparently normal EGFP-labeled neurons were observed in L2 (at P6 and P20). In contrast to the normal and control animals (i.e., nonelectroporated hemisphere or electroporated with only EGFP), those in which *NT-3* was overexpressed showed distinct bundles in L1. There was also an unusually dense dendritic plexus in L1a (Fig. 4*B*). In the same animals, EGFP-expressing neurons were evident in L2 in adjoining parietal and auditory cortex (Fig. 4*C,D*). In these areas, some patchiness of dendrites was discerned, but the main effect of the NT-3 seemed to be a pronounced thickening of the dendritic plexus in L1a.

In order to visualize the complete population of dendrites from all layers, we counterstained 5 brains with MAP2, a global

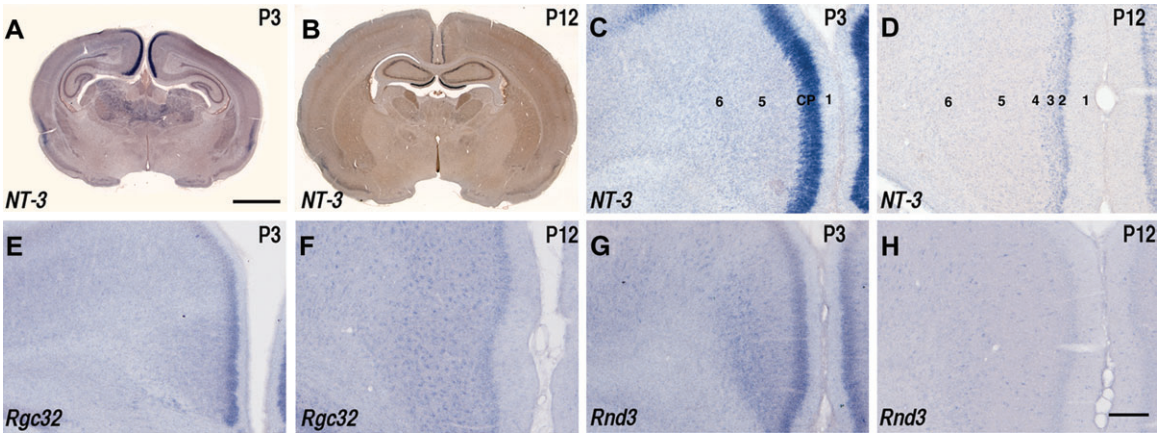

Figure 3. In situ hybridizations of 3 selected genes at P3 and at P12 (*A–D*) Expression of *NT-3* shows strong signals in L2 of GRS at P3 (*A* and, higher magnification, *C*) but less strong at P12 (*B* and, higher magnification, *D*). (*E*, *F*) Expression of *Rgc-32* in L2 of GRS at P3 (in *E*) and at P12 (in *F*). (*G*, *H*) Expression of *Rnd3* in L2 of GRS at P3 (in G) and at P12 (in *H*). Labels in *C* and *D* indicate layers and cortical plate (CP) and can be extrapolated to *E–H*. Scale bars = 2 mm in *A* for *A* and *B*; 200 μm in *H*, for *C–H*.

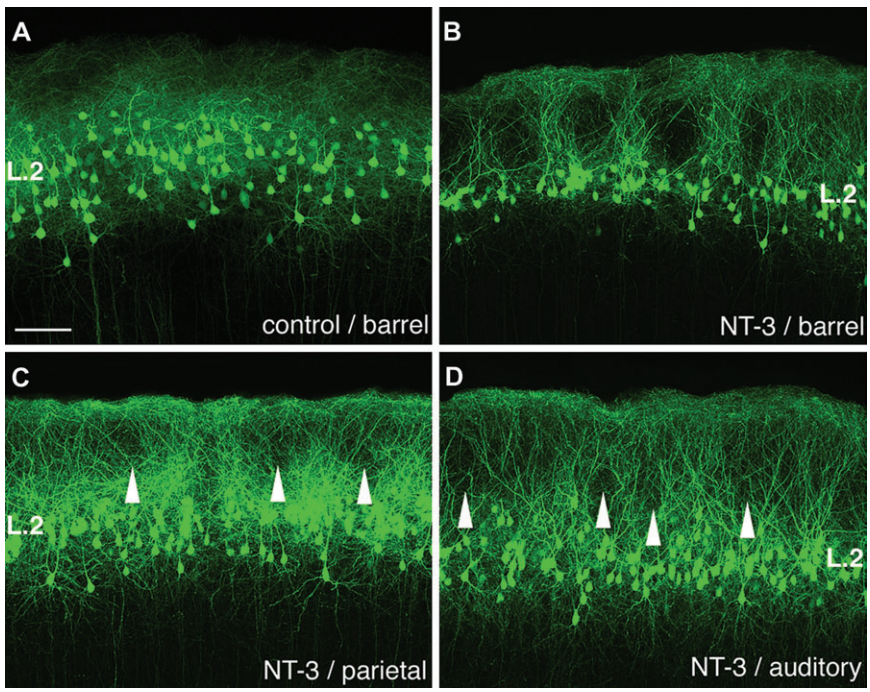

Figure 4. Ectopically expressed NT-3 induces dendritic bundles in neocortical L1. (*A*) EGFP-expressing L2 pyramidal neurons at P20, after electroporation of EGFP alone at E18. Note uniform distribution of cells and dendrites, without bundles. (*B*) Electroporation of *EGFP* and *NT-3* at E18 induces distinct dendritic bundles in barrel cortex. (*C*, *D*) Bundles and interbundle spaces (arrowheads) are discernible in other areas, after similar intervention (electroporation at E18). These are less distinct than in BF, but a conspicuous patchiness, corresponding to dendritic tufts, is evident in L1a. Parietal (*C*) and auditory (*D*) cortices, both at P20. Scale bar = 100 μm.

dendritic marker. In the electroporated hemisphere, dense MAP2 staining was evident in L1, but this had a distinct alternation of dense and less dense zones. The dense regions coincided with the induced bundles, and the less dense zones coincided with interbundle spaces (Fig. 5). Interbundle spaces (between the EGFP-labeled dendrites from L2) may largely contain distal tufts of L5 apical dendrites. In the contralateral (nonelectroporated) hemisphere and in hemispheres electroporated with EGFP alone, MAP2-ir was overall less dense and, in particular, was evenly distributed within L1 (Fig. 5). The configuration of MAP2-positive dendrites in the deeper layers appeared similar in brains electroplated with either *NT-3/EGFP* or *EGFP* alone. After calbindin immunohistochemistry, laminar patterns were judged as normal in the *NT-3*–overexpressed hemisphere (Supplementary Fig. S4).

Other Effects of Overexpression of NT-3

To test for possible effects of NT-3 on thalamocortical connectivity, we counterstained 5 brains with anti-VGluT2 antibody, a global marker for thalamocortical terminals (Fujiyama et al. 2001; Kaneko and Fujiyama 2002; Kaneko et al. 2002). In the BF of *NT-3*–electroporated animals, VGluT2-ir was distinctly patchy, with dense zones interdigitating with the ectopically induced dendritic bundles in L1 (Fig. 6). In the control, contralateral (nonelectroporated) hemisphere, the band of VGluT2-ir was thinner in L1a, without any discernible periodicity.

In tangentially sectioned BF, induced bundles formed a prominent honeycomb in L1 (Fig. 7). The bundle size (100–200 μm wide) is much larger than that of the classic bundles of L5 neurons but about the same dimension as the L2-derived bundles in the GRS (Wyss et al. 1990). As in the GRS, cell bodies did not form obvious patches. PV-ir in normal BF forms a micromodular honeycomb at the border of L1 and L2 (Fig. 7 and Fig. 11 in Ichinohe, Fujiyama, et al. 2003). Double labeling for PV-ir and EGFP-ir revealed that the PV honeycomb overlaps with the L2 dendritic bundles (Fig. 7). No alteration, in thickness or staining intensity, was noticed in the PV honeycomb between experimental and normal brains.

Single Neuron Morphology after Overexpression of NT-3

We prepared nonfixed tissue slices of BF in order to evaluate dendritic phenotype at the level of single neurons. Before intracellular filling, electrophysiology was carried out to control for cell viability and assess membrane-firing properties. All neurons were found to be regular spiking, regardless of whether they were in the experimental hemisphere (n = 16 cells; 3 animals, P24–26), the contralateral nonelectroporated hemisphere (n = 8 cells; 1 animal, P27), or normal, nonelectroporated brains (n = 9 cells; 1 animal, P25).

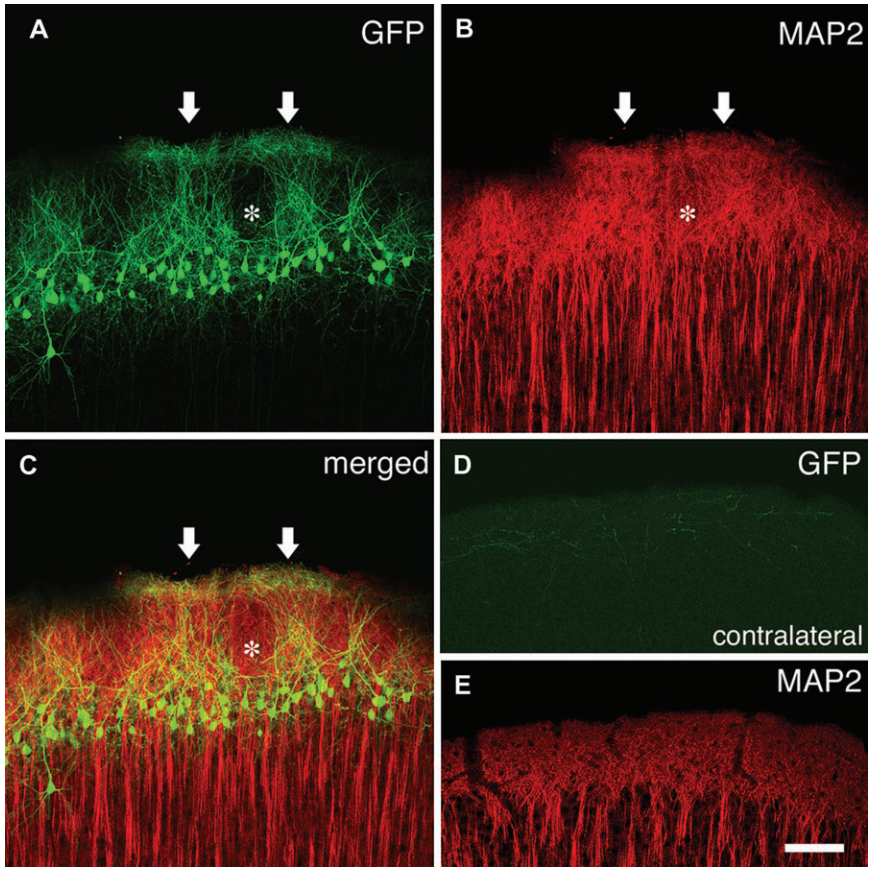

Figure 5. Dendritic neuropil of barrel cortex, with and without electroporation of *NT-3*. (*A*) Ectopically expressed NT-3 (at E18) induces prominent bundles (arrows) and interbundles (at asterisk), labeled with EGFP. (*B*) Dendritic neuropil, labeled by MAP2 immunofluorescence. Denser patches (arrows) and sparser (asterisk) are evident in L1. (*C*) Merged image: NT-3–induced, EGFP-positive dendritic bundles (arrows) correspond to zones of denser MAP2-ir labeling. (*D*, *E*) The contralateral (nonelectroporated) hemisphere has no EGFP-labeled elements in L1 and there is no periodicity in the MAP2 labeling in L1. This is also thinner. Scale bar = 100 μm.

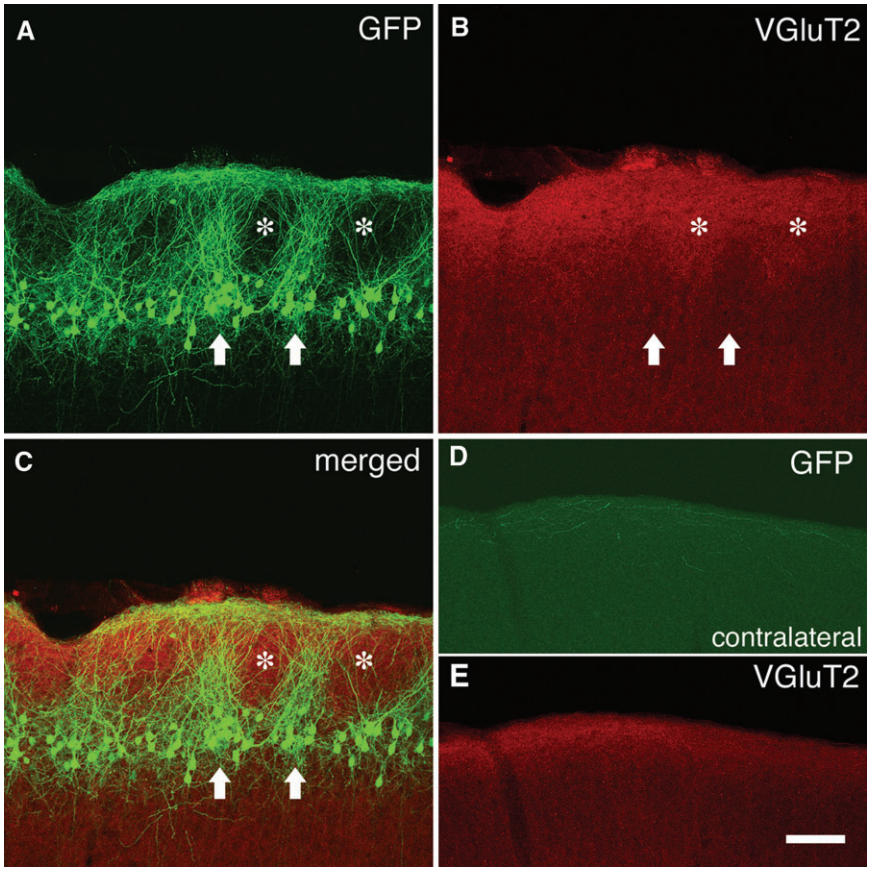

Figure 6. Overexpression of NT-3 (at E18, BF) results in atypical patchiness of thalamocortical terminations in L1. (*A*) Dendritic bundles (P20), induced by ectopically expressed NT-3 (arrows) and interbundles (asterisk) labeled with EGFP. (*B*) VGluT2 imunofluorescence reveals an abnormally thick and patchy plexus in L1 (dense patches, asterisk; interpatches, arrows). (*C*) Merged image: interbundle spaces (asterisk) are occupied by VGluT2-labeled profiles. (*D*, *E*) The contralateral (nonelectroporated) hemisphere is EGFP negative (*D*) and has a thinner, uniform VGluT2-positive plexus in L1. Scale bar = 100 μm.

Biocytin was injected intracellularly. Subsequent histochemistry for streptavidin–Alexa 594 showed a range of dendritic morphologies but no clear qualitative differences as regards number of dendrites, dendritic orientation, or degree of spininess. However, further quantitative analysis revealed several differences (Fig. 8), consistent with previous reports from culture preparations that NT-3 influences dendritic outgrowth.

To investigate differences between *NT-3*-expressing and normal cells ($n = 9$ NT-3 group; $n = 10$ control group), confocal images were stacked, and dendritic complexity was analyzed by using Neurolucida software. We found that the 2 groups were distinguishable by Sholl analysis. In particular, this showed an increased dendritic complexity (branching) for *NT-3*-expressing neurons in a 50- to 200-μm zone from the cell body. In this zone, the average number of dendritic intersections was 13.2 (control) versus 23.4 (*NT-3* expressing), and the range of dendritic intersections was 4.8–25.7 (for control) and 7.8–36.6 (for *NT-3* expressing). The longest dendritic branch was also longer for *NT-3*-expressing cells (510 μm from the soma) than for control (400 μm).

In addition, we scored the number of dendrites reaching into L1a (where both MAP2 and EGFP revealed a thickened dendritic plexus in the experimental animals), in relation to soma depth. In our in vitro intracellular fills, *NT-3*-expressing cells were at 128–440 μm from the pia surface and normal cells were at 111–324 μm. We analyzed cells lying between 200 and 300 μm because this represented the majority of the *NT-3*-expressing cells ($n = 10$ of 16, NT-3 group; $n = 6$ of 17, control group). For *NT-3*-expressing cells, 4 to 20 dendrites were found superficially in L1a (average: 10.8 dendrites) In contrast, for the control group, the range was 0–6 dendrites (average: 4 dendrites).

Discussion

Dendritic bundles have been moderately well characterized anatomically as consisting of a core of L5 apical dendrites (Escobar et al. 1986; Peters and Kara 1987; White and Peters 1993) or, according to a more recent study, interdigitating systems from L5 and L2 (Ichinohe, Fujiyama, et al. 2003). Not all L5 dendrites form into bundles ("singletons" Peters and Kara 1987 and reviewed in Rockland and Ichinohe 2004), and dendrites from L4 and L6 have been considered apart. A recent in vitro investigation, where bundles were visualized in EGFP mice, failed to find convincing evidence for an underlying neuronal circuitry restricted to anatomically defined boundaries (Krieger et al. 2007). Alternate possibilities, then, include a more complex anatomical arrangement whereby physiological columnarity emerges from substructures yet to be identified or that the functional significance of bundles has not been optimally formulated (Krieger et al. 2007). The controlled induction of dendritic bundles, as reported here, offers a new in vivo model for investigating mechanisms of

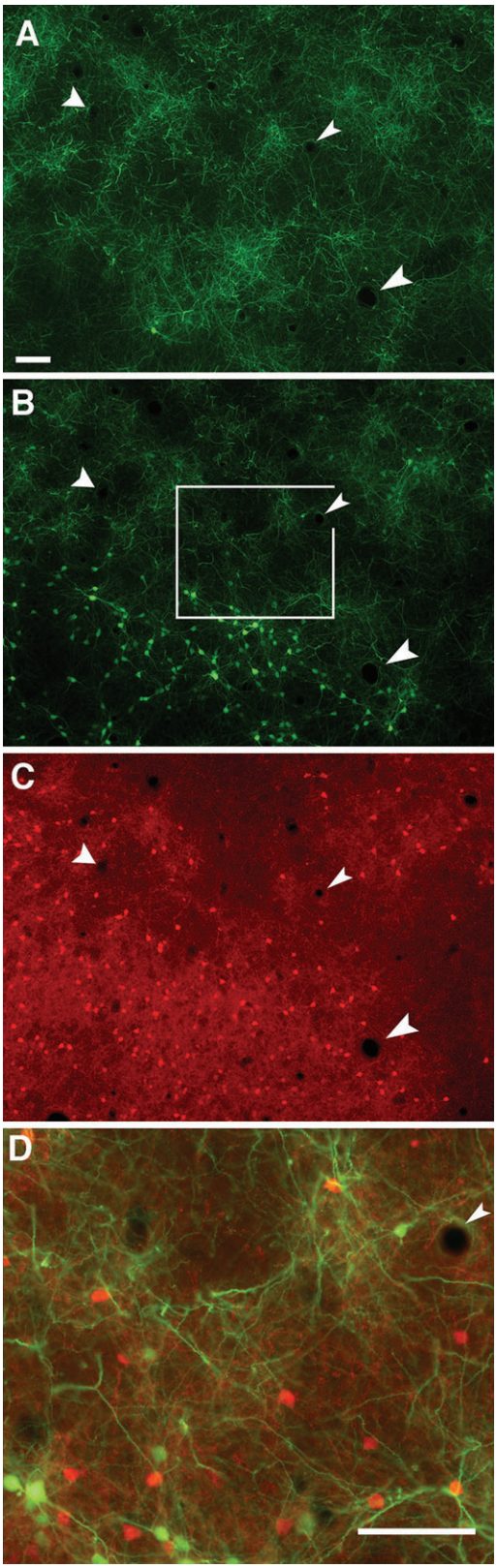

Figure 7. Tangential sections to show PV-ir honeycomb and NT-3–induced dendritic bundles in L1 of BF. (*A*, *B*) Sequential tangential sections (40-μm thickness) from L1 of BF. EGFP-positive dendritic bundles were evident as patches in upper (*A*) and lower (*B*) sections. (*C*) PV-ir patches from same section as (*B*), showing honeycomb micromodularity at the border of L1 and L2. (*D*) Higher magnification merge from inset in (*B*). EGFP and PV staining can be seen as largely overlapping. Arrowheads indicate same blood vessels. Scale bar = 100 μm in *A* for *A*–*C*; 100 μm in *D*.

bundle formation, as well as basic issues of their network circuitry and area and species specialization.

By using microarray analysis, we identified genes that are highly expressed in L2 of the rat GRS at P3 (preceding dendritic bundle formation). Stage-specific comparison (GRS L2, P3 vs. P12) identified a very large number of genes (306), consistent with the multiplicity of developmentally related processes ongoing during the first postnatal week. Microarray data clearly spotlighted the differential genetic profile of GRS L2 versus L2 of BF (173 genes expressed at a 2-fold higher level in GRS at P3) and GRS L2 versus GRS L5 (107 genes expressed at a 2-fold higher level in L2 at P3). This approach also revealed that the preferentially high expression of *NT-3* in GRS L2 was transient from P3 to P12, coinciding with the period of bundle formation, as previously identified (Ichinohe, Yoshihara, et al. 2003). The transient expression of *NT-3* in GRS had been remarked after in situ hybridization studies in rat (Friedman et al. 1991), as well as mouse (Vigers et al. 2000). In mouse, *NT-3* expression is reported as more specific to L3 and as persisting, albeit at reduced levels after P8, into adulthood (8 wk and, more weakly, 20 wk). This may be a species difference between mouse and rat, and we note that L2 dendritic bundles are much less distinct in the mouse GRS (N. Ichinohe and K.S. Rockland, personal observation).

A causal role for NT-3–mediated events in bundle formation was supported by the successful induction of L2 bundles in BF, an area where these are normally absent. These bundles are relatively large (100–200 μm wide), in the same size range as L2 bundles in GRS (Wyss et al. 1990). NT-3 has previously been reported to influence neurite outgrowth in vitro and at the level of single neurons (McAllister et al. 1995; Catapano et al. 2004), but this is the first report that NT-3 is involved in bundle formation.

Role of NT-3

NT-3 is a secreted protein, with multiple functions related to neurite development and maintenance (Ghosh and Greenberg 1995; McAllister et al. 1995; Catapano et al. 2001, 2004). It is known to influence dendritic outgrowth in vitro (McAllister et al. 1995; Catapano et al. 2004). Intracellularly filled neurons in our electroporated hemispheres showed dendritic changes (i.e., increased branching and elongation) consistent with this effect. How overexpression of NT-3 influences bundle formation is less clear.

In tissue culture, PC12 cells are known to respond to NT-3 with neurite outgrowth (Tsoulfas et al. 1993). This response is attributed to an interaction of NT-3 with the TrkC receptor, and it is well established that interactions of NT-3 and TrkC activate multiple intracellular signaling cascades, including the mitogen activated protein kinase (MAPK) pathway (Kaplan and Miller 1997, 2000). However, although *TrkC* is highly expressed in the GRS L2 at P3, its expression level is also high in L2 of BF, and the expression level in both areas is stable over time. The mechanisms underlying bundle formation are thus likely to be ligand dependent. An additional observation is that our microarray data show *DUSP6* as having a similar expression pattern as *NT-3* in the developing GRS L2. DUSP6 is known to specifically inactivate MAPK activity (Keyse 2008). From this, we can infer that specific inactivation of downstream MAPK pathways may be important for dendritic bundle formation by DUSP6. The relationship between DUSP6 and NT-3/TrkC is unclear.

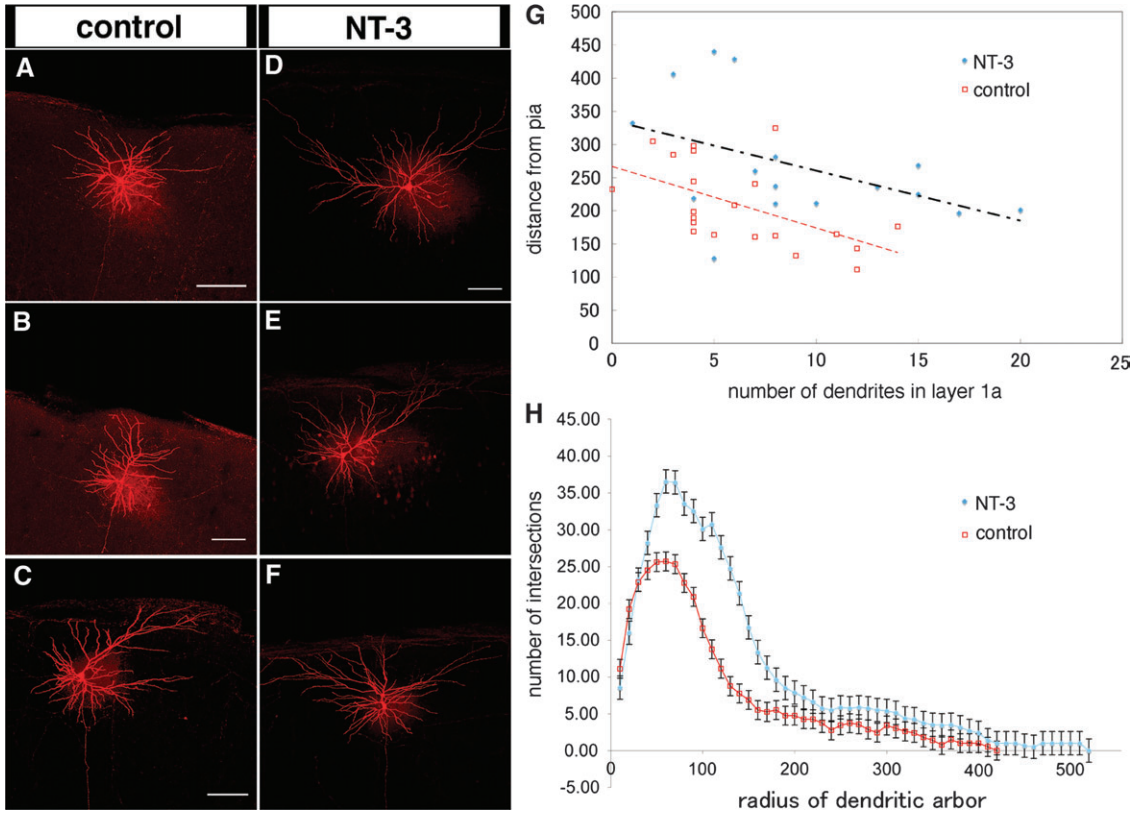

Figure 8. Morphometric analysis of dendrites of biocytin-filled neurons in L2. Confocal images of biocytin-filled L2 neurons from BF of control (*A–C*) and NT-3–overexpressing (*D–F*) brains. Scale bars = 100 μm in *D* for *D–F*. (*G*) Scatter plot shows number of dendrites that extend into L1a (*x*-axis) in relation to soma depth (*y*-axis). (*H*) Sholl analysis of control ($n = 10$) and NT-3–overexpressing ($n = 9$) cells. Number of dendritic intersection points (*y*-axis) in relation to circles of increasing radius (*x*-axis).

The partial spatial and temporal coincidence of NT-3 and TrkC expression raises the possibility that NT-3 acts cell autonomously for dendritic bundle formation in L2. Double staining for MAP2 and electroporated EGFP, however, showed that a population of NT-3/EGFP–negative dendrites are also involved in the induced dendritic bundles in BF L2. Another factor nonsupportive of an exclusively cell-autonomous mechanism is that NT-3 usually influences target cells nonautonomously by being secreted from other cells (Genc et al. 2004).

NT-3 is also implicated in the establishment of synaptic interactions between thalamic axons and cortical neurons (Ma et al. 2002; Hanamura et al. 2004). Another possibility, therefore, is that the prominence of dendritic bundles in the upper layers is associated with or even secondary to changes in thalamocortical inputs. In our electroporated hemispheres, the thalamic plexus in L1 (from ventral posterior medial nucleus [VPm] and posterior nucleus [PO]) was abnormally thickened and patchy. Terminal patches interdigitated with the induced dendritic bundles in BF, suggestive of a chemorepulsant effect on L2 dendrites. This pattern is opposite to what occurs in the GRS, where thalamocortical terminations from the anterior nucleus colocalize with L2 dendritic bundles (Wyss et al. 1990; Ichinohe et al. 2008). *TrkC* is strongly expressed in the anterior nucleus (but not VPm or PO; Hassink et al. 1999) and may be supposed to have an attractant influence for the *NT-3*–expressing bundles.

A previous in vitro study using slices of P14 ferret visual cortex showed that dendritic growth and differentiation are regulated by neurotrophins in a layer-specific manner. In that study, NT-3 enhanced dendritic complexity mainly in L6 neurons (McAllister et al. 1995), but the authors excluded neurons in L2 and L3 because these had not yet migrated to their final position. In our study, MAP2-ir in the deeper layers is indistinguishable between *NT-3*–electroporated hemispheres and controls (Supplementary Fig. S4). Thus, we suggest that NT-3 effects were localized, as intended by the electroporation, to L2 or L2 and 3. Other possible secondary induced effects were not identified, but further detailed analyses of dendritic structure and other cellular and subcellular features would be desirable.

Other Factors in Bundle Formation

Neurite guidance and orientation are influenced by complex homophilic and heterophilic interactions and regulation of multiple signaling cascades (Tessier-Lavigne and Goodman 1996; Whitford et al. 2002).

1. Cell adhesion molecules, including cadherins, have been implicated in neurite outgrowth and synapse formation (Hirano et al. 2003; Arikkath and Reichardt 2008). In our screening and selection process, no cell adhesion molecules were selected (we note that *Fath*, cadherin family cell adhesion molecule, showed high and specific expression in GRS L2 during the period of bundle formation but could not meet the strict criteria of selection at step 3), but *Rnd3*, a member of the Rho family of small GTP-binding proteins (Chardin 2006), was found to be transiently expressed in GRS L2 before dendritic bundle formation. In fibroblast and epithelial cells, Rnd3 protein colocalizes with cadherins in adherens junctions (Nobes et al. 1998). Several cadherins are

reported to be expressed in a layer-specific manner in GRS, but expression is throughout the postnatal development (Bekirov et al. 2002). It may be that Rnd3 has an important role in the specialization of L2 GRS, acting together with cadherins. OCAM, a cell adhesion molecule of the IgG superfamily located on the dendritic surface of L5 neurons, has been specifically implicated in the formation of L2 dendritic bundles in the GRS (see Introduction). OCAM expression in neocortical areas is less clear-cut, and its possible role in bundle formation in areas outside the GRS requires further investigation.

2. There is an obvious temporal coincidence between the epoch of formation of L2 bundles (from P5 in the GRS and [induced bundles] from P6 in BF, the date of earliest sacrifice) and the stage of gap junction coupling among pyramidal neurons (Peinado et al. 1993; Rorig and Sutor 1996; Montoro and Yuste 2004; Sutor and Hagerty 2005). Gap junctions might contribute to bundle formation by intercellular exchange of signaling molecules or by synchronization of firing, but there has so far been no evidence for the existence of gap junctions between dendrites in L2 bundles. Our microarray data showed no stage-specific or site-specific changes in the expression level of 6 gap-junction related molecules (i.e., *Cx32*, *Cx36*, *Cx40*, *Cxn37*, *Gja1*, *Gja3*), although a seventh (*Gjb2*) showed an increased expression level from P3 to P12 (data not shown). Our microarray screening did show a transient expression of *Rnf182* (ring finger protein, E3 ubiquitin ligase), specific to the GRS L2. Rnf182 protein physically interacts with ATP6V0C (ATPase, H+ transporting, lysosomal 16Kda, V0 subunitC; Liu et al. 2008). ATP6V0C is known as a key component for its role in the formation of gap junction complex and neurotransmitter release channels (Finbow et al. 1994; Morel 2003). Future experiments might investigate the involvement of gap junctions in L2 dendritic bundle formation through degradation of ATP6V0C by Rnf182.
3. Dendritic outgrowth and pattern formation require significant cytoskeletal remodeling (Threadgill et al. 1997; Whitford et al. 2002), which is presumably important in bundle formation as well. Cytoskeletal changes result from a wide variety of extrinsic factors, intrinsic codes, and cascades of signaling factors and transcriptional regulators (Gallo and Letourneau 2000; Wong and Ghosh 2002). These would include not only *NT-3* but also other genes identified as highly and specifically expressed in L2 GRS at P3 (i.e., *Neuropilin*, *DUSP6*, *Rnd3*).
4. Additional candidate factors include several other systems that form patches in the uppermost layers and thalamocortical terminations in L1, the PV honeycomb, In rat visual cortex, a transiently patchy serotonergic innervation has been reported (Nakazawa et al. 1992), and bundle formation may likely result from complex interactions of multiple factors.

"Rewired" Hybrid Areas

The GRS and BF, respectively a limbic and primary sensory cortex, are distinguished by many features. Particularly relevant for the present results, L2 is a conspicuously cell-dense layer in GRS, but in BF, it is less prominent and is often grouped together with subjacent L3 ("L2/3"). After overexpression of *NT-3*, no changes were apparent in the density or grouping of cells in L2, and firing properties were normal (i.e., regular spiking). The dendritic morphometry of individual neurons in L2 was slightly but not dramatically altered from the normal phenotype. Dendritic spines and intrinsic axon collateralization appeared normal. The main discernible effect of overexpressing *NT-3*, therefore, was the ectopic bundle formation, along with an influence on the distal dendritic and thalamocortical plexus in L1a. Pups were grossly normal, and no changes were observed in onset or nature of whisking. (We note, however, that electroporation was unilateral in all cases.)

Auditory and parietal areas were also modified as a result of electroporated *NT-3*. In these areas, changes were most noticeable in the thickness of the dendritic and thalamic plexus in L1a, but some tendency for dendritic bundles could be discerned in L2. The less pronounced bundles could be owing to technical factors; that is, pulsed current was targeted to BF, so that bordering areas received lesser, subthreshold levels of *NT-3*.

Conclusion

The ectopic expression of distinct L2 dendritic bundles offers a new in vivo model for investigating cortical bundle formation, connectivity, and function, and dendritic and modular reactions to experimental, developmental, or pathological changes. This can be considered a variant paradigm of "rewired" cortex. Continued experiments might probe for finer connectional effects subsequent to the spatial reorganization of L2 and apply this technique to other layers or areas.

Supplementary Material

Supplementary Tables S1–S5 and Figures S1–S4 can be found at: http://www.cercor.oxfordjournals.org/.

Funding

Grant-in-Aid for Young Scientists from the Japan Society for the Promotion of Science (19700303 to T.M.); Grant-in-Aid for Scientific Research on Priority Areas "System study on higher order brain functions" from the Ministry of Education, Culture, Sports, Science and Technology, Japan (17024064, 18020032, 18500270 to N.I.); Joint Research Programs of the National Institute for Basic Biology Japan; Internal Research Fund of RIKEN Brain Science Institute (to K.S.R.).

Notes

The authors would like to thank Ms Yoshiko Abe, Ms Hiromi Mashiko, and Mr James Hyde for their excellent technical assistance, Drs Yoshinobu Sugitani and Tomomi Shimogori for their technical advice for in utero electroporation, and Drs Yumiko Hatanaka and Junichi Miyazaki for pCAGGS plasmid. *Conflict of Interest*: None declared.

Address correspondence to Toshio Miyashita, PhD, Laboratory for Cortical Organization and Systematics, RIKEN Brain Science Institute, 2-1 Hirosawa, Wako-shi, Saitama 351-0198, Japan. Email: tmiyashita@berkeley.edu.

References

Arikkath J, Reichardt LF. 2008. Cadherins and catenins at synapses: roles in synaptogenesis and synaptic plasticity. Trends Neurosci. 31: 487–494.

Badea TC, Niculescu FI, Soane L, Shin ML, Rus H. 1998. Molecular cloning and characterization of RGC-32, a novel gene induced by

complement activation in oligodendrocytes. J Biol Chem. 273:26977–26981.
Bekirov IH, Needleman LA, Zhang W, Benson DL. 2002. Identification and localization of multiple classic cadherins in developing rat limbic system. Neuroscience. 115:213–227.
Berbel P, Auso E, Garcia-Velasco JV, Molina ML, Camacho M. 2001. Role of thyroid hormones in the maturation and organisation of rat barrel cortex. Neuroscience. 107:383–394.
Catapano LA, Arlotta P, Cage TA, Macklis JD. 2004. Stage-specific and opposing roles of BDNF, NT-3 and bFGF in differentiation of purified callosal projection neurons toward cellular repair of complex circuitry. Eur J Neurosci. 19:2421–2434.
Catapano LA, Arnold MW, Perez FA, Macklis JD. 2001. Specific neurotrophic factors support the survival of cortical projection neurons at distinct stages of development. J Neurosci. 21: 8863–8872.
Chardin P. 2006. Function and regulation of Rnd proteins. Nat Rev Mol Cell Biol. 7:54–62.
Cooper BG, Mizumori SJ. 2001. Temporary inactivation of the retrosplenial cortex causes a transient reorganization of spatial coding in the hippocampus. J Neurosci. 21:3986–4001.
DeFelipe J. 2005. Reflections on the structure of the cortical minicolumn. Neocortical modularity and the cell minicolumn. New York: Nova Biomedical Books. p. 57–92.
Escobar MI, Pimienta H, Caviness VS, Jr, Jacobson M, Crandall JE, Kosik KS. 1986. Architecture of apical dendrites in the murine neocortex: dual apical dendritic systems. Neuroscience. 17:975–989.
Feldman ML, Peters A. 1974. A study of barrels and pyramidal dendritic clusters in the cerebral cortex. Brain Res. 77:55–76.
Finbow ME, Goodwin SF, Meagher L, Lane NJ, Keen J, Findlay JB, Kaiser K. 1994. Evidence that the 16 kDa proteolipid (subunit c) of the vacuolar H(+)-ATPase and ductin from gap junctions are the same polypeptide in Drosophila and Manduca: molecular cloning of the Vha16k gene from Drosophila. J Cell Sci. 107(Pt 7):1817–1824.
Fleischhauer K. 1974. On different patterns of dendritic bundling in the cerebral cortex of the cat. Kidney Int. 5:115–126.
Friedman WJ, Ernfors P, Persson H. 1991. Transient and persistent expression of NT-3/HDNF mRNA in the rat brain during postnatal development. J Neurosci. 11:1577–1584.
Fujiyama F, Furuta T, Kaneko T. 2001. Immunocytochemical localization of candidates for vesicular glutamate transporters in the rat cerebral cortex. J Comp Neurol. 435:379–387.
Gallo G, Letourneau PC. 2000. Neurotrophins and the dynamic regulation of the neuronal cytoskeleton. J Neurobiol. 44:159–173.
Genc B, Ozdinler PH, Mendoza AE, Erzurumlu RS. 2004. A chemoattractant role for NT-3 in proprioceptive axon guidance. PLoS Biol. 2:e403.
Ghosh A, Greenberg ME. 1995. Distinct roles for bFGF and NT-3 in the regulation of cortical neurogenesis. Neuron. 15:89–103.
Hanamura K, Harada A, Katoh-Semba R, Murakami F, Yamamoto N. 2004. BDNF and NT-3 promote thalamocortical axon growth with distinct substrate and temporal dependency. Eur J Neurosci. 19:1485–1493.
Harker KT, Whishaw IQ. 2002. Impaired spatial performance in rats with retrosplenial lesions: importance of the spatial problem and the rat strain in identifying lesion effects in a swimming pool. J Neurosci. 22:1155–1164.
Hassink GC, van Esseveldt KE, Dijkhuizen PA, Verhaagen J, Boer GJ. 1999. Ontogeny of neurotrophin receptor trkC expression in the rat forebrain and anterior hypothalamus with emphasis on the suprachiasmatic nucleus. Neuroscience. 92:705–712.
Hatanaka Y, Hisanaga S, Heizmann CW, Murakami F. 2004. Distinct migratory behavior of early- and late-born neurons derived from the cortical ventricular zone. J Comp Neurol. 479:1–14.
Hatanaka Y, Murakami F. 2002. In vitro analysis of the origin, migratory behavior, and maturation of cortical pyramidal cells. J Comp Neurol. 454:1–14.
Hirano S, Suzuki ST, Redies C. 2003. The cadherin superfamily in neural development: diversity, function and interaction with other molecules. Front Biosci. 8:d306–d355.
Ichinohe N, Fujiyama F, Kaneko T, Rockland KS. 2003. Honeycomb-like mosaic at the border of layers 1 and 2 in the cerebral cortex. J Neurosci. 23:1372–1382.
Ichinohe N, Knight A, Ogawa M, Ohshima T, Mikoshiba K, Yoshihara Y, Terashima T, Rockland KS. 2008. Unusual patch matrix organization in the retrosplenial cortex of the reeler mouse and shaking rat Kawasaki. Cereb Cortex. 18:1125–1138.
Ichinohe N, Yoshihara Y, Hashikawa T, Rockland KS. 2003. Developmental study of dendritic bundles in layer 1 of the rat granular retrosplenial cortex with special reference to a cell adhesion molecule, OCAM. Eur J Neurosci. 18:1764–1774.
Jones EG. 2000. Microcolumns in the cerebral cortex. Proc Natl Acad Sci U S A. 97:5019–5021.
Kaneko T, Fujiyama F. 2002. Complementary distribution of vesicular glutamate transporters in the central nervous system. Neurosci Res. 42:243–250.
Kaneko T, Fujiyama F, Hioki H. 2002. Immunohistochemical localization of candidates for vesicular glutamate transporters in the rat brain. J Comp Neurol. 444:39–62.
Kaplan DR, Miller FD. 1997. Signal transduction by the neurotrophin receptors. Curr Opin Cell Biol. 9:213–221.
Kaplan DR, Miller FD. 2000. Neurotrophin signal transduction in the nervous system. Curr Opin Neurobiol. 10:381–391.
Keyse SM. 2008. Dual-specificity MAP kinase phosphatases (MKPs) and cancer. Cancer Metastasis Rev. 27:253–261.
Konishi T. 2004. Three-parameter log normal distribution ubiquitously found in cDNA microarray data and its application to parametric data treatment. BMC Bioinformatics. 5:5.
Konishi T. 2006. Detection and restoration of hybridization problems in affymetrix GeneChip data by parametric scanning. Genome Inform. 17:100–109.
Konishi T. 2008. Data distribution of short oligonucleotide expression arrays and its application to the construction of a generalized intellectual framework. Stat Appl Genet Mol Biol. 7Article 25.
Krieger P, Kuner T, Sakmann B. 2007. Synaptic connections between layer 5B pyramidal neurons in mouse somatosensory cortex are independent of apical dendrite bundling. J Neurosci. 27:11473–11482.
Liu QY, Lei JX, Sikorska M, Liu R. 2008. A novel brain-enriched E3 ubiquitin ligase RNF182 is up regulated in the brains of Alzheimer's patients and targets ATP6V0C for degradation. Mol Neurodegener. 3:4.
Lucio RA, Garcia JV, Ramon Cerezo J, Pacheco P, Innocenti GM, Berbel P. 1997. The development of auditory callosal connections in normal and hypothyroid rats. Cereb Cortex. 7:303–316.
Ma L, Harada T, Harada C, Romero M, Hebert JM, McConnell SK, Parada LF. 2002. Neurotrophin-3 is required for appropriate establishment of thalamocortical connections. Neuron. 36:623–634.
McAllister AK, Lo DC, Katz LC. 1995. Neurotrophins regulate dendritic growth in developing visual cortex. Neuron. 15:791–803.
Miyashita T, Nishimura-Akiyoshi S, Itohara S, Rockland KS. 2005. Strong expression of NETRIN-G2 in the monkey claustrum. Neuroscience. 136:487–496.
Miyashita T, Rockland KS. 2007. GABAergic projections from the hippocampus to the retrosplenial cortex in the rat. Eur J Neurosci. 26:1193–1204.
Montoro RJ, Yuste R. 2004. Gap junctions in developing neocortex: a review. Brain Res Brain Res Rev. 47:216–226.
Morel N. 2003. Neurotransmitter release: the dark side of the vacuolar-H+ATPase. Biol Cell. 95:453–457.
Mountcastle VB. 1997. The columnar organization of the neocortex. Brain. 120(Pt 4):701–722.
Mountcastle VB. 2003. Introduction. Computation in cortical columns. Cereb Cortex. 12:2–4.
Nakazawa M, Koh T, Kani K, Maeda T. 1992. Transient patterns of serotonergic innervation in the rat visual cortex: normal development and effects of neonatal enucleation. Brain Res Dev Brain Res. 66:77–90.
Niwa H, Yamamura K, Miyazaki J. 1991. Efficient selection for high-expression transfectants with a novel eukaryotic vector. Gene. 108:193–199.
Nobes CD, Lauritzen I, Mattei MG, Paris S, Hall A, Chardin P. 1998. A new member of the Rho family, Rnd1, promotes disassembly of

actin filament structures and loss of cell adhesion. J Cell Biol. 141:187–197.
Peinado A, Yuste R, Katz LC. 1993. Gap junctional communication and the development of local circuits in neocortex. Cereb Cortex. 3:488–498.
Peters A, Kara DA. 1987. The neuronal composition of area 17 of rat visual cortex. IV. The organization of pyramidal cells. J Comp Neurol. 260:573–590.
Rockland KS, Ichinohe N. 2004. Some thoughts on cortical minicolumns. Exp Brain Res. 158:265–277.
Rorig B, Sutor B. 1996. Regulation of gap junction coupling in the developing neocortex. Mol Neurobiol. 12:225–249.
Saito T, Nakatsuji N. 2001. Efficient gene transfer into the embryonic mouse brain using in vivo electroporation. Dev Biol. 240:237–246.
Sutor B, Hagerty T. 2005. Involvement of gap junctions in the development of the neocortex. Biochim Biophys Acta. 1719:59–68.
Tabata H, Nakajima K. 2001. Efficient in utero gene transfer system to the developing mouse brain using electroporation: visualization of neuronal migration in the developing cortex. Neuroscience. 103:865–872.
Tessier-Lavigne M, Goodman CS. 1996. The molecular biology of axon guidance. Science. 274:1123–1133.
Threadgill R, Bobb K, Ghosh A. 1997. Regulation of dendritic growth and remodeling by Rho, Rac, and Cdc42. Neuron. 19:625–634.
Tsoulfas P, Soppet D, Escandon E, Tessarollo L, Mendoza-Ramirez JL, Rosenthal A, Nikolics K, Parada LF. 1993. The rat trkC locus encodes multiple neurogenic receptors that exhibit differential response to neurotrophin-3 in PC12 cells. Neuron. 10:975–990.
Vigers AJ, Baquet ZC, Jones KR. 2000. Expression of neurotrophin-3 in the mouse forebrain: insights from a targeted LacZ reporter. J Comp Neurol. 416:398–415.
White EL, Peters A. 1993. Cortical modules in the posteromedial barrel subfield (Sml) of the mouse. J Comp Neurol. 334:86–96.
Whitford KL, Dijkhuizen P, Polleux F, Ghosh A. 2002. Molecular control of cortical dendrite development. Annu Rev Neurosci. 25:127–149.
Wong RO, Ghosh A. 2002. Activity-dependent regulation of dendritic growth and patterning. Nat Rev Neurosci. 3:803–812.
Wyss JM, Van Groen T. 1992. Connections between the retrosplenial cortex and the hippocampal formation in the rat: a review. Hippocampus. 2:1–11.
Wyss JM, Van Groen T, Sripanidkulchai K. 1990. Dendritic bundling in layer I of granular retrosplenial cortex: intracellular labeling and selectivity of innervation. J Comp Neurol. 295:33–42.